

Effect of porosity and kerogen distribution on elastic properties of Bazhenov formation shale rocks – Rock physics modeling

© 2025 A.I. Tyapkina¹, I.A. Berezina², G.A. Kalmykov¹,
V.S. Okunevich², I.O. Bayuk²

¹ *Lomonosov Moscow State University, Moscow, Russia*

² *Schmidt Institute of Physics of the Earth, Russian Academy of Sciences, Moscow, Russia*

Corresponding author: I.O. Bayuk, e-mail: ibayuk@ifz.ru

Abstract. A parametric anisotropic rock physics (petroelastic) model of kerogen-rich shale rocks of Bazhenov formation is constructed. The model is built based on the rock's microstructure and composition provided by the scanning electron microscopy and mineral-component model obtained from well logs interpretation. The proposed model considers that kerogen can be found in different forms in the mineral matrix: isometric inclusions and thin layers. Besides, the model allows one to distribute the porosity between kerogen and mineral matrix. A sensitivity analysis of the model to its parameters shows that the distribution of kerogen between the matrix and layers can lead to significant changes in the velocities of elastic waves (up to 1.5 times for compression waves and up to 4 times for shear waves). The velocities are also highly sensitive to the porosity distribution between kerogen and matrix. The constructed petroelastic model is applied to invert the distribution of the following parameters from well log data: (a) kerogen in the mineral matrix, (b) kerogen in thin layers, (c) matrix porosity, and (d) kerogen porosity.

Ключевые слова: rock physics, petroelastic modeling, anisotropy, elastic properties, Bazhenov formation, shale, kerogen porosity, matrix porosity, unconventional reservoir rocks

Cite this article as: Tyapkina A.I., Berezina I.A., Kalmykov G.A., Okunevich V.S., Bayuk I.O. Effect of porosity and kerogen distribution on elastic properties of Bazhenov formation shale rocks – Rock physics modeling, *Seismicheskie Pribory*, 2025, vol. 61, no. 1, pp. 14–35. (in Russian). <https://doi.org/10.21455/si2025.1-2>

Introduction

The Bazhenov formation (BF) draws attention in the oil and gas industry in recent years, since this black shale formation is actively explored as an additional source of hydrocarbons. The knowledge of shale's petrophysical and mechanical properties is valuable for the effective oil production from this type of unconventional reservoir with hydraulic fracturing. The petroelastic modeling for shale rocks is a potent tool for predicting physically consistent reservoir properties for this purpose.

Many researchers have modeled the effective elastic properties of oil and gas shales throughout the world [Hornby *et al.*, 1994; Jakobsen *et al.*, 2003; Dræge *et al.*, 2006; Bayuk *et al.*, 2007, 2008; Ortega *et al.*, 2007; Bandyopadhyay, 2009; Sayers, 2013; Vasin *et al.*, 2013; Zhao *et al.*, 2016]. Their works differ in rock-physics modeling strategies associated with the both methods and representation of the complex multiscale structure particularly anisotropy of shales. This anisotropy is usually characterized as a transversely isotropic type with

a vertical axis of symmetry (VTI). It often results from horizontal layering as a consequence of uniform sedimentation, and also from the presence of oriented fractures and microcracks, lenses of organic matter (kerogen), and particles of clay minerals. Another specific feature of shales is that these rocks exhibit multiscale porous space structure from nanopores in mature organic matter to macropores due to dissolution of silica minerals. These factors and also multi-component mineral composition led to complex petroelastic models.

In this work, we construct a multiscale rock-physics model for the Bazhenov formation oil shale based on data provided by well logs and core analysis. Bazhenov oil formation is represented by organic-rich laminated siliceous fine-grained rocks and shares the key characteristics with other major producing formations such as Barnett, Bakken etc.

Based on the microstructure observation, we assume that shale studied in this work is composed of the isotropic kerogen-clay-silica matrix with silt-size inclusions. Besides the rock contains kerogen flakes and lenses that have preferred horizontal orientation which results in VTI anisotropy of the formation.

The main goal of the present work is to quantify the influence of kerogen morphology and porosity types on the elastic wave velocities. To achieve this goal, we construct a multi-step rock-physics model. In this model, the kerogen morphology is represented by three forms differing in size including elongated lenses, dispersed thin inclusions, and isometrical silt-size particles (in dissolved radiolaria skeleton). The last two types of kerogen are considered as inclusions in a matrix which may be in a contact or isolated. In this case to estimate the kerogen effect on the effective elastic properties of shale the classical self-consistent [Berryman, 1980, 1995] and Kuster–Toksöz [Kuster, Toksöz, 1974a,b] methods are applied. To simulate effect of the kerogen lenses we use the Backus averaging [Backus, 1962]. This method allows us to treat the shale as a medium with mineral layers and kerogen microlayers. We consider two main types of oil-filled pores – organic pores in the kerogen and non-organic pores in the matrix. The rock physics modeling requires a construction of a hierarchical volumetric model that allows us to obtain a distribution of volume concentration of minerals, kerogen, and pores inserted at each step of the petroelastic model construction.

A sensitivity analysis of the constructed model provides us a reasonable choice of valuable parameters. The analysis shows that for fixed values of kerogen content and total porosity the distribution of the kerogen between the matrix and layers and distribution of porosity between the kerogen and matrix can considerably change the elastic wave velocities (up to several times).

We apply our model to well log data and invert the distribution of (a) kerogen amount between matrix and layers and (b) oil porosity between kerogen and matrix. When solving this problem we pay attention to non-uniqueness of the inverse problem solution and demonstrate how wide the solution domain could be.

Composition and microstructure of Bazhenov formation shale rocks

In this section we analyze rock samples of the studied formation drilled from a well focusing on their microstructure and mineral composition. The latter is particularly important as it forms the basis for building a geologically reliable conceptual model.

Rock composition and fabric

The mixture of siliceous mudstones and mudstones rocks compose the Bazhenov Shale formation in the studied well. The most common types in the interval are biomorphic siliceous mudstones (radiolarites), argillaceous and kerogen-rich siliceous mudstones. The integration of X-ray diffraction method, X-ray fluorescence method, pyrolytic analysis, as well as

nuclear magnetic resonance (NMR) and Formation Microimaging (FMI) logs allows us to determine a detailed mineral composition [Balushkina *et al.*, 2014]. It is quite similar to other shale's mineralogies especially to lower Barnett shale formation [Loucks, Ruppel, 2007; Gamero-Diaz *et al.*, 2012; Speight, 2020]. The rock composition includes the following components (Fig. 1): silica, clay minerals, carbonates, pyrite, organic matter, and feldspar. Silica minerals are represented by quartz and chalcedony, along with lesser amounts of opal. These minerals appear as recrystallized radiolaria's skeletons and are locally common as amorphous phase. The overall silica content is about 34%. Clay minerals are dominantly illite and kaolinite.

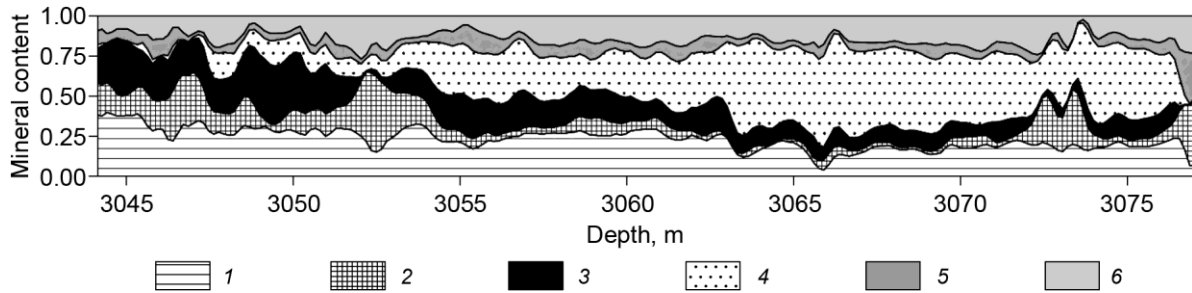


Fig. 1. Bazhenov rock composition in the studied well

1 – clays; 2 – carbonates; 3 – kerogen; 4 – silica; 5 – pyrite-feldspar; 6 – porosity

The clay platelets are randomly oriented. This loss of preferred orientation could be due to presence of higher amounts of silt content [Gipson, 1966; Curtis *et al.*, 1980]. The clay component in BF shale rocks does not exceed 40 %, in average 20 %. It is interesting that the albite content (ranging from 0 % to 35 %) correlates with the amount of clay minerals in the study formation [Balushkina, Kalmykov, 2016].

Kerogen of the BF rocks occurs both as dispersed matter in the matrix and as lenses or flakes with preferred orientation (fig. 2), forming the fabric anisotropy. The kerogen volume concentration is high (as compared to shale rocks of other known formations) with typical value around 20 %. The Rock-Eval analysis showed that the kerogen belongs to type II.

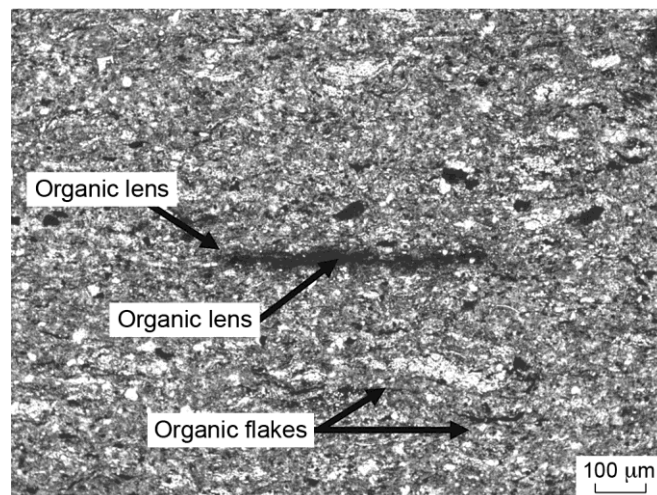


Fig. 2. Organic matter (OM) in Bazhenov formation shale rock

Pyrite is present in the framboidal forms, which indicates its authigenic nature. However, pyrite replacement of radiolarians is locally observed (Fig. 3, a). The pyrite volume concentration can reach 8 %.

The carbonate component of these rocks is shown in Fig. 3, *b*. It is represented largely by calcite and dolomite, and slightly by siderite and ankerite. The primary carbonates are mostly in the forms of shell detritus, bivalve shells, teutids, foraminifera, coccolithophorids, belemnites, and their remains. The secondary carbonate's minerals are formed due to the replacement of siliceous material of the radiolaria's skeletons [Balushkina, Kalmykov, 2016]. Calcite-replaced radiolarians are also met (fig 3, *b*).

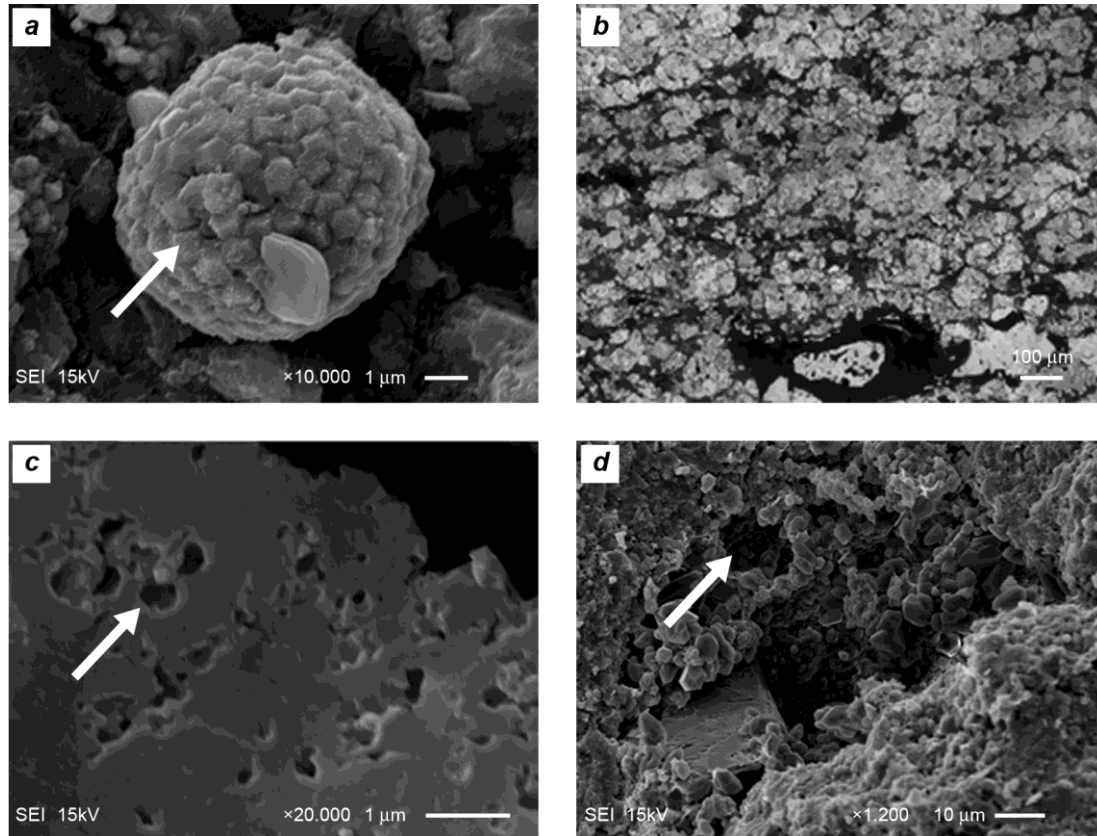


Fig. 3. SEM images of Bazhenov formation shale (photos from [Kalmykov, 2016])

a – pyrite replacement of radiolarian; *b* – calcite-replaced radiolarians; *c* – isometric pores in the kerogen; *d* – quartz grains with intercrystalline porosity and intraform pores

Porous space

The analysis of thin sections and SEM photos provides a characteristics of rock's porous space. The primary porosity was lost during compaction, cementation, and infilled by organic matter. The secondary porosity could be divided into two types referred as organic and non-organic porosity. Organic porosity or kerogen porosity is formed by isometric pores with size up to 2 μm (Fig. 3, *c*). Commonly, they are interconnected by small lenses of organic matter. This type of porosity has appeared at the end of the primary petroleum forming zone due to kerogen maturation. Non-organic pores are typically much larger than pores in kerogen. They represent intraparticle and intercrystalline porosity. Intraform voids formed due to a dissolution of radiolarians shell are dominant and reach up to 200 microns size (Fig. 3, *d*). The recrystallization process of opal into chalcedony (or less often into quartz) and the pyritization of organic matter (OM) and porous space has led to occurrence of the intercrystalline porosity (Fig. 3, *d*). Open porosity measured with kerosene on the core samples varies from 1.0 % to 2.59 % and the well-log derived total porosity range is from 3 % to 27 % (Fig. 4).

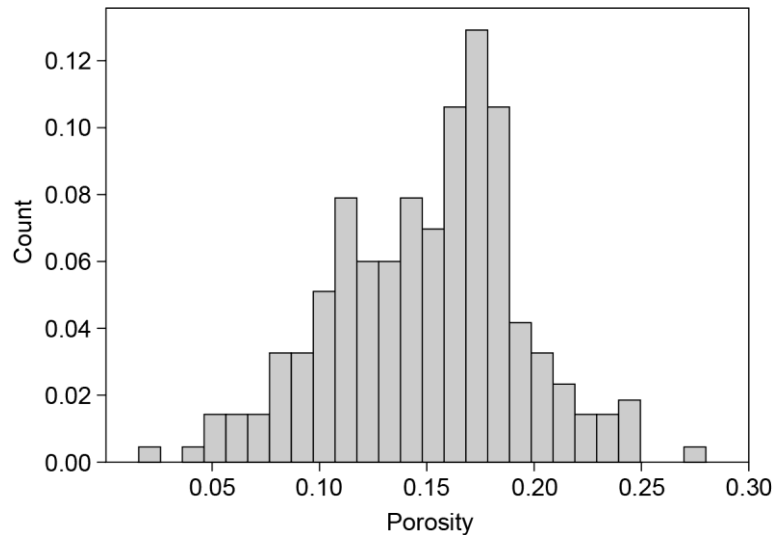


Fig. 4. Histogram of total porosity derived from NMR log

Petroelastic model of Bazhenov formation shale rocks

Mathematical model of effective physical properties

A mathematical model of effective physical properties of rocks including BF shale rocks (petroelastic model) is designed in three stages (Fig. 5). The first stage is a construction of so-called “model medium” that mimics specific features of the rock microstructure. The model medium includes the mineral grains, pores, and fractures whose shape is approximated by ellipsoids of revolutions having various aspect ratio. The second stage involves a parametrization of the model which means a revealing of parameters that characterize the physical properties of components and microstructural parameters controlling rock’s physical properties. Then, at the third stage, a suitable rock-physics method is selected to calculate the effective physical properties of the model from its parameters. The theoretical values of physical properties are compared with experimental ones. If the discrepancy between the values is higher than an accepted level the model is corrected [Chesnokov *et al.*, 2010; Bayuk, Tikhotskiy, 2018].

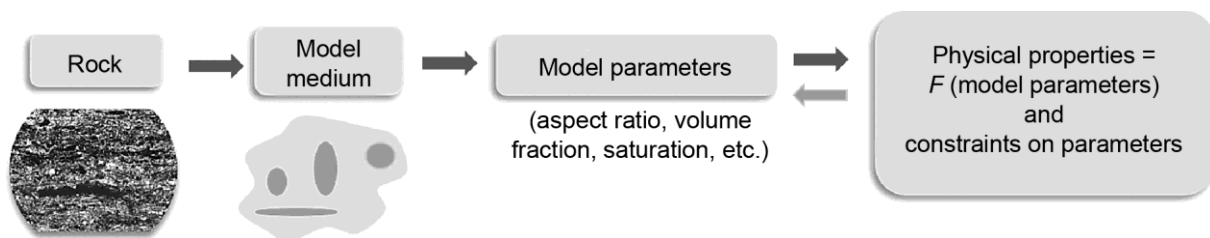


Fig. 5. Mathematical model of effective physical properties of rock

A basic principle for constructing a petroelastic model is “going from small to larger heterogeneities”. First the effective physical properties are calculated for a medium consisting from the smallest inclusions. Then, inclusions of larger size are imbedded in this medium [Danko *et al.*, 2017].

Construction of hierarchical petroelastic model of BF shales

The Bazhenov formation shale rocks exhibit rather complicated hierarchical microstructure. Consequently, the model medium is not too simple and should reflect its general specific features. The steps for constructing the hierarchical petroelastic model of Bazhenov formation shales are as follows (Fig. 6):

Step 1. Oil-saturated pores are inserted in kerogen matrix and the result of the first step is the porous kerogen.

Step 2. Silica, porous kerogen, and clay particles are mixed. We considered clay particles as spherical inclusions having isotropic properties. Strictly speaking this is not correct, since the clay minerals are anisotropic, and clay platelets have non-isometric shape and

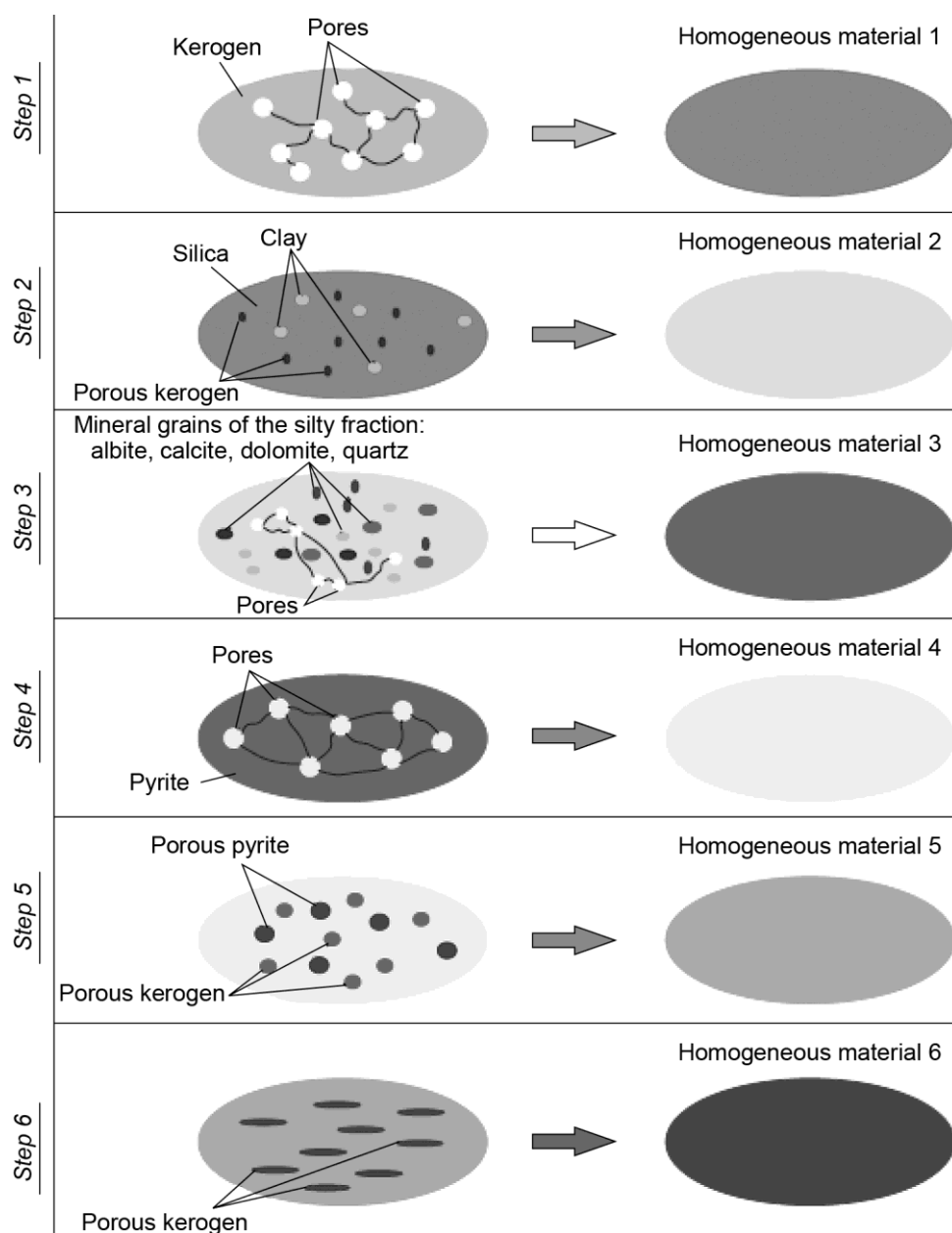


Fig. 6. Hierarchical petroelastic model of Bazhenov formation shale rocks

commonly aligned [Bayuk *et al.*, 2008]. However, in this study we used this assumption for simplicity since our goal is to analyze the influence of the following factors on the effective elastic properties: (a) distribution of porosity between the kerogen and mineral matrix and (b) distribution of porous kerogen between inclusions in the matrix and layers. Besides, the elastic moduli of the stiffness matrices of clay and silica are not dramatically different. Thus, the results of sensitivity study of the constructed model demonstrate that the effective properties of our model are slightly dependent on the clay particle shape that varies from 10^{-4} to 0.1. This also can be explained by that the maximum clay content does not exceed 25 % in the rocks which is not too high.

Note that in a modeling that is aimed to study the factors controlling the anisotropy of effective physical properties of rock the clay mineral anisotropy and non-spherical shape of clay platelets should be taken into account.

In our case, isotropic medium (we call it Material 2) obtained at this step significantly simplifies our further modeling.

Step 3. Mesopores and silt-size minerals are embedded in Material 2 that is considered as a matrix. We call the resulting medium Material 3.

Step 4. Adding isometric saturated pores in pyrite. As a result, Material 4 is obtained. Note that in the modeling we fill the pyrite-related pores with formation water, however the result will not significantly change if the pores are filled with oil or oil-water mixture.

Step 5. Porous pyrite and porous kerogen (in dissolution voids of radiolaria skeletons) are inserted in Material 3. The resulting medium with effective properties is called Material 5.

Step 6. Oriented elongated lenses of porous kerogen are added in Material 5 thereby producing anisotropy in resulting elastic properties of the studied Bazhenov formation shale rocks.

At steps 1, 2, 4, and 5 the effective elastic properties are calculated with the use of self-consistent (SCA) method [Berryman, 1980, 1995]. For step 3 the Kuster–Toksöz method [Kuster, Toksöz, 1974a,b] is applied since mesopores and silt-size minerals seem to be rather isolated. To calculate the effective elastic properties of the resulting medium (step 6) the oriented elongated kerogen lenses are considered as layers and the Backus method [Backus, 1962] is applied. The elastic properties of components composing the rocks and used for the modeling are listed in Table 1 with respective references. The bulk modulus of oil and formation water is taken as 1.3 and 2.8 GPa, respectively, and their densities are 0.85 and 1.1 g/cm³.

Table 1. Elastic moduli and densities of components used for modeling

Component	K , GPa	μ , GPa	ρ , g/cm ³	Reference
Kerogen	3.5	1.75	1.2	[Yan, Han, 2013]
Silica	23.0	23.0	2.65	[Bayuk <i>et al.</i> , 2019]
Clay	21.0	7.0	2.58	[Berge, Berryman, 1995]
Dolomite	71.5	34.2	2.86	[McSkimin <i>et al.</i> , 1965]
Albite	56.8	28.4	2.62	[Belikov <i>et al.</i> , 1970]
Calcite	75.4	30.4	2.71	[Peselnick, Robie, 1963]
Quartz	37.8	43.7	2.65	[McSkimin <i>et al.</i> , 1965]
Pyrite	142.8	125.5	5.02	[Ahrens, 1995]

Hierarchical volumetric model of studied rocks

This section presents a method for calculating the volume concentrations of components constituting the petroelastic model which are inserted at each step of the model construction. The concentration of a component inserted at each step is indicated by c_{np} , where n is the step number and p is the index of the corresponding component. The following indices of compo-

nents are used: *k* for kerogen, *oil* for oil, *cl* for clay, *sil* for silica, *dol* for dolomite, *alb* for albite, *cal* for calcite, *qz* for quartz, *pyr* for pyrite, and *wat* for water. For example, c_{1k} is the volume concentration of kerogen at the 1st step (construction of oil-saturated porous kerogen), c_{1oil} is the volume concentration of oil in kerogen at the 1st step. Notation like b_i is used for the total composition of the *i*-th step, and all these values are equal to 1. This notation serves only as an indicator of the material obtained at the *i*-th step for the model construction at the next steps. Thus, notation c_{6b5} means volume concentration of material with the effective properties obtained at step 5, when kerogen layers are introduced into this medium at the final sixth stage; c_{6b1} is the volume concentration of oil-saturated kerogen layers.

The system of equations for the volume concentrations of the components inserted at each step has the form:

$$\text{step 1:} \quad c_{1k} + c_{1oil} = b_1 = 1; \quad (1)$$

$$\text{step 2:} \quad c_{2b1} + c_{2cl} + c_{2sil} = b_2 = 1; \quad (2)$$

$$\text{step 3:} \quad c_{3b2} + c_{3dol} + c_{3alb} + c_{3cal} + c_{3qz} + c_{3oil} = b_3 = 1; \quad (3)$$

$$\text{step 4:} \quad c_{4pyr} + c_{4wat} = b_4 = 1; \quad (4)$$

$$\text{step 5:} \quad c_{5b3} + c_{5b1} + c_{5b4} = b_5 = 1; \quad (5)$$

$$\text{step 6:} \quad c_{6b5} + c_{6b1} = b_6 = 1, \quad (6)$$

where c_{1k} , c_{1oil} , c_{2b1} , c_{2cl} , c_{2sil} , c_{3b2} , c_{3dol} , c_{3alb} , c_{3cal} , c_{3qz} , c_{3oil} , c_{4pyr} , c_{4wat} , c_{5b3} , c_{5b1} , c_{5b4} , c_{6b5} , c_{6b1} are the sought-for volume concentrations of rock-forming components inserted at each step. Equations (1)–(6) contain 18 unknown variables.

We express b_1 , b_2 , b_3 , b_4 , and b_5 in equations (1)–(5) in terms of concentrations and substitute them into equation (6). As a result, we obtain the following equation:

$$c_{6b5} \left\{ c_{5b3} \left[c_{3b2} (c_{2b1} (c_{1k} + c_{1oil}) + c_{2cl} + c_{2sil}) + c_{3dol} + c_{3alb} + c_{3cal} + c_{3qz} + c_{3oil} \right] + \right. \\ \left. + c_{5b1} (c_{1k} + c_{1oil}) + c_{5b4} (c_{4pyr} + c_{4wat}) \right\} + c_{6b1} (c_{1k} + c_{1oil}) = 1. \quad (7)$$

Since the total volume concentration of minerals, kerogen, and fluids in the rock is given (we have so-called mineral-component model), additional relationships that follow from equation (7) can be used to calculate the concentration of each component:

$$\text{kerogen:} \quad c_{6b5} c_{5b3} c_{3b2} c_{2b1} c_{1k} + c_{6b5} c_{5b1} c_{1k} + c_{6b1} c_{1k} = v_k, \quad (8)$$

$$\text{oil:} \quad c_{6b5} c_{5b3} c_{3b2} c_{2b1} c_{1oil} + c_{6b5} c_{5b3} c_{3oil} + c_{6b5} c_{5b1} c_{1oil} = v_{oil}, \quad (9)$$

$$\text{clay:} \quad c_{6b5} c_{5b3} c_{3b2} c_{2cl} = v_{cl}, \quad (10)$$

$$\text{silica:} \quad c_{6b5} c_{5b3} c_{3b2} c_{2sil} = v_{sil}, \quad (11)$$

$$\text{dolomite:} \quad c_{6b5} c_{5b3} c_{3b2} c_{2dol} = v_{dol}, \quad (12)$$

$$\text{albite:} \quad c_{6b5} c_{5b3} c_{3b2} c_{2alb} = v_{alb}, \quad (13)$$

$$\text{calcite:} \quad c_{6b5} c_{5b3} c_{3b2} c_{2cal} = v_{cal}, \quad (14)$$

$$\text{quartz:} \quad c_{6b5} c_{5b3} c_{3b2} c_{2qz} = v_{qz}, \quad (15)$$

$$\text{pyrite:} \quad c_{6b5} c_{5b4} c_{4pyr} = v_{pyr}, \quad (16)$$

$$\text{water:} \quad c_{6b5} c_{5b4} c_{4wat} = v_{wat}, \quad (17)$$

where v_k , v_{oil} , v_{cl} , v_{sil} , v_{dol} , v_{alb} , v_{cal} , v_{qz} , v_{pyr} , v_{wat} are the known volume fractions of kerogen, oil, clay, silica, dolomite, albite, calcite, quartz, pyrite, and water provided by the mineral-component model derived from a petrophysical study or log data.

As a result, we have a system of 16 independent equations (1)–(6) and (8)–(18) and 18 unknowns. This system underdetermined and has many solutions. Moreover, equations (8)–(17) are nonlinear. Formally, such a system of equations can be solved numerically using

18 nested loops for each parameter, and many sets of concentrations can be selected as solutions. However, this approach is practically unrealizable due to the enormous computational time required to execute such an algorithm. In order to minimize computational costs, we use all possible relationships between the concentrations of the components, which makes it possible to reduce the number of unknowns to 7 (and as a result, to implement only 7 nested loops in the solution algorithm). For, example, using the ratio between the volume concentration of minerals at step 3 we express the quartz, calcite, and albite concentrations via the dolomite concentration. Similar substitution is made for clay and silica concentrations at step 2. We also use all of equations (1)–(6) in order to reduce the number of nested cycles. Besides, in order to decrease the computation time, we use bounds for volume concentrations of fluid-filled voids at steps 1 and 4 as 50 %. This gives a possibility to exit the respective cycles much earlier. Steps in the volume concentration values and a permissible discrepancy between the sought-for and given concentrations for different components provided by the mineral-component model are selected based on reasonable computation time.

The chosen admissible misfit between the sought-for and given total volume concentrations of mineral, kerogen, and fluids is 2 %, and the step in concentrations is 1.5 %. In what follows we call the method of determining the volume concentration of components inserted at different steps “construction of hierarchical volume model”.

Before going to step 6 a necessity of such a complicated modeling (steps 1–5) was justified. To do this we build a one-step model where all heterogeneities are mixed simultaneously, and the self-consistent method of Berryman is used for calculating the effective elastic properties of the mixture. Our modeling show that the velocities calculated from the one-step effective moduli are greatly overestimated compared to those obtained in the 5-step modeling (see Table 2). The basic values of parameters used for the modeling are listed in Table 3 of the next section. As a result, to reach the experimental velocities around 40 % of kerogen should be added in lenses. However, this amount is abnormally high compared to the real volume concentration of kerogen in the whole rock (not greater than 25 %). Thus, to obtain reliable velocities the proposed many-step modeling is necessary.

Table 2. Effective elastic moduli and calculated for many-step and one-step models

Model type	Bulk modulus, GPa	Shear modulus, GPa	V_p , km/s	V_s , km/s
Many-step model	12.4	7.7	3.11	1.81
One-step model	27.3	20.0	4.81	2.93

Sensitivity study of petroelastic model

After the model construction an analysis of the model sensitivity to its parameters should be performed. In order to do this, we vary each parameter within a specified range with a selected step. The analysis is carried out for the model parameters shown in Table 3 in accordance with ranges of their variability. The ranges are approximately selected after the visual analysis of thin sections. The basic values correspond to the average mineral composition of the studied rocks. A visual analysis of microstructure allows us to approximately estimate the most common values of morphological parameters. The basic values are fixed when sensitivity of other parameters is studied. Note that at steps 1, 2, 4, 5, and 6 the volume concentration of respective component is given for the considered step while the sum of volume concentration of all components of this step is 100 %. For example, kerogen porosity 20 % at step 1 means that other 80 % of volume is occupied by kerogen.

Table 3. Basic values of parameters and their ranges used for sensitivity study (100 % means that kerogen is matured to oil)

Model parameter	Basic value, %	Range, %
Kerogen porosity (step 1)	40	0–100
Porous kerogen (step 2)	30	0–80
Clay (step 2)	20	0–50
Silica (step 2)	50	0–80
Matrix porosity (not in kerogen and pyrite, step 3)	8	0–30
Albite (step 3)	7	
Calcite (step 3)	5	
Dolomite (step 3)	5	
Pyrite porosity (step 4)	15	5–30
Pyrite (step 5)	8	
Porous kerogen (step 5)	1.5	0–50
Porous kerogen (step 6)	5	0–30

Sensitivity study to the kerogen porosity

Here and below, other model parameters are fixed and their values are shown in Table 3. Figure 7 shows the components of effective stiffness tensor versus kerogen porosity. Up to porosity of 60 %, the components C_{11} , C_{33} , and C_{44} decrease more intensive compared to their behavior at the greater porosity. The value 60 % can be considered as a “critical porosity value” when the fluid in pores becomes connected.

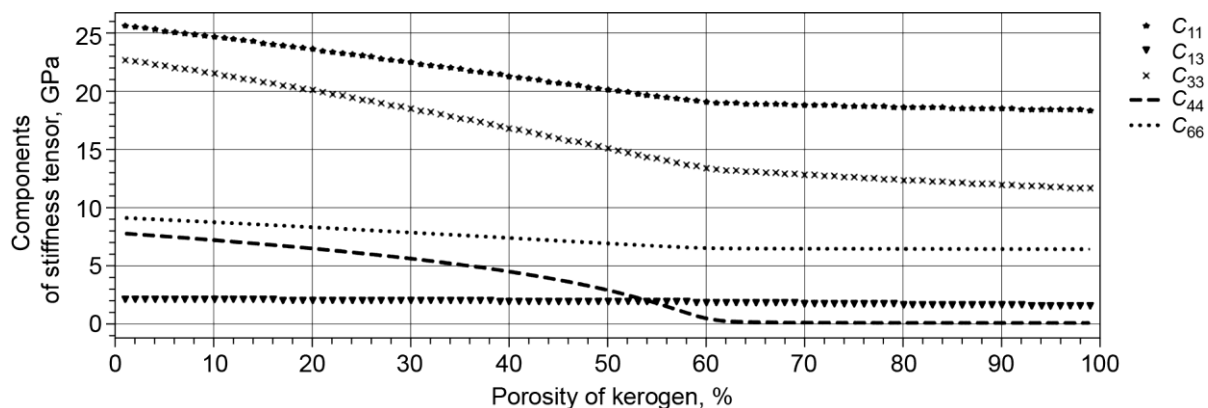
**Fig. 7.** Change in the effective moduli C_{ij} depending on porosity in kerogen at the step 1

Figure 8 demonstrates dependences of elastic wave velocities V_P , V_{SH} , and V_{SV} on the wavefront direction for different kerogen porosity. The direction is counted from the vertical axis that coincides with the symmetry of effective stiffness matrix of the rock (VTI). As seen, V_P and V_{SV} may decrease almost twice as the kerogen porosity grows from 10 % to 60 %.

Sensitivity of the model to the increasing concentration of matrix kerogen (inserted at step 2)

This study is performed in two ways: (1) decreasing of silica and (2) decreasing of clay content. Kerogen is porous. Note that kerogen, clay, and silica are the most abundant substances in the studied rocks. The volume concentrations of other minerals – quartz, albite, pyrite, calcite, and dolomite, and kerogen porosity are taken as shown in Table 3. The calculated

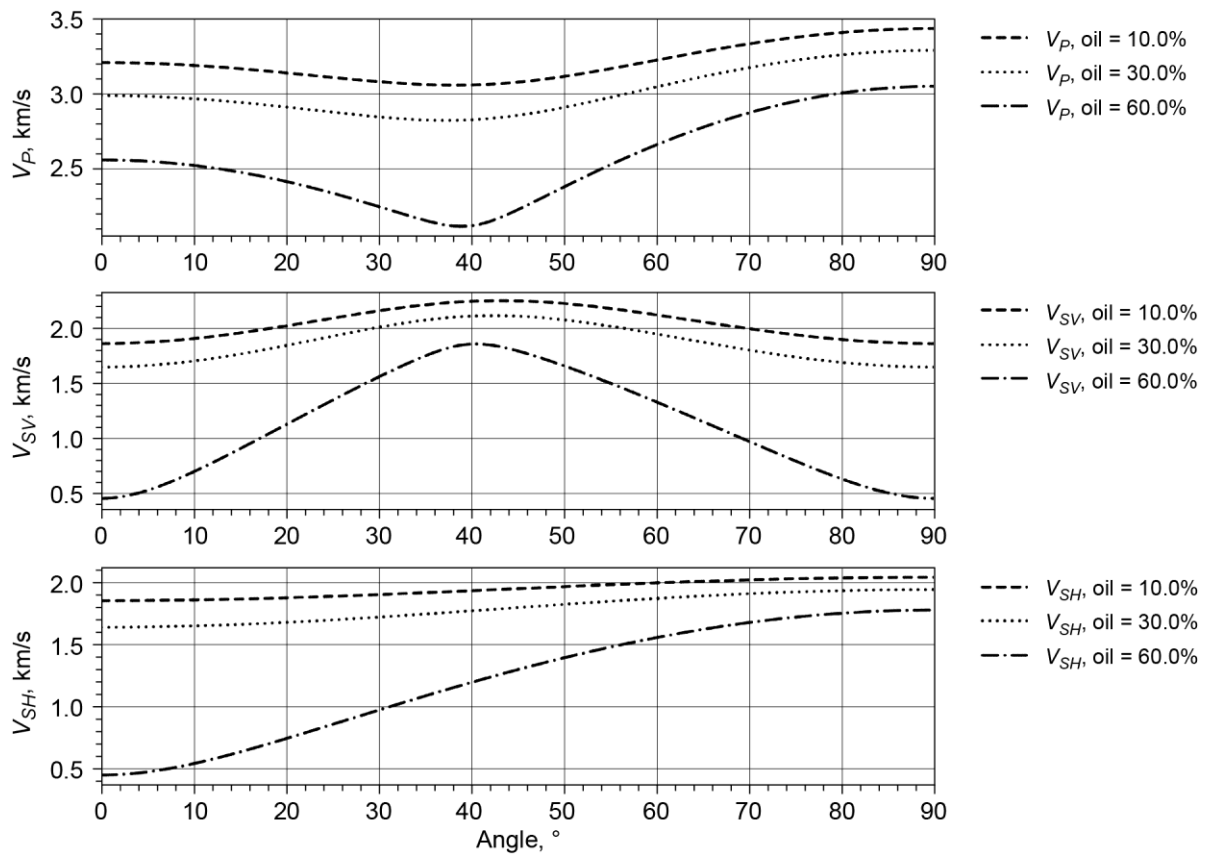


Fig. 8. Angular dependences of velocities V_P , V_{SH} , and V_{SV} on kerogen porosity of 10 %, 30 %, and 60 % after the 6th step. The angle is counted from the vertical symmetry axis. The volume concentrations of porous kerogen at respective step of modeling (2nd, 5th, and 6th) are as follows: $v_2^k = 0.30$, $v_5^k = 0.015$, $v_6^k = 0.05$

effective moduli at step 2 are demonstrated in Figures 9 and 10. As seen, for kerogen concentration up to about 25 % the effective elastic moduli are greater if the kerogen replaces silica compared to the case when kerogen replaces clay. This behavior is due to the fact that the concentration of the “softest” component (kerogen) is small, and the effect of the most rigid component (silica) dominates. Then, another behavior is observed – kerogen becomes to dominate and changes the moduli in a way specific for each replaced substance.

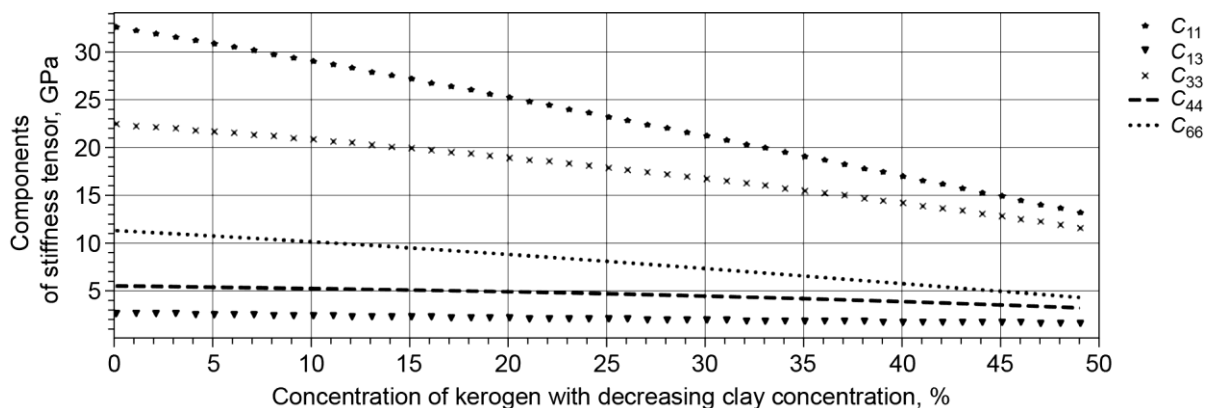


Fig. 9. Change in effective moduli C_{ij} after 6th step with an increase in kerogen concentration due to decreasing of clay at the step 2

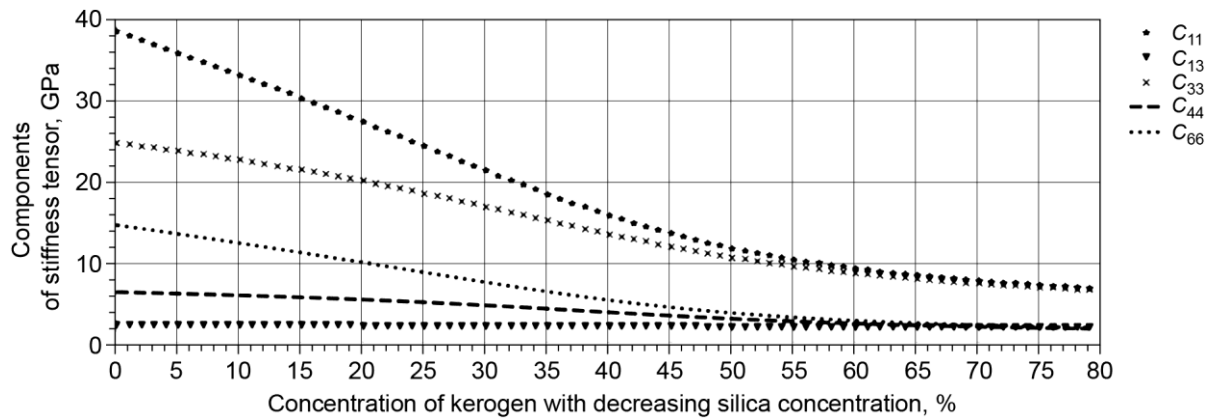


Fig. 10. Change in effective modules C_{ij} after 6th step with an increase in kerogen concentration due to decreasing of silica at step 2

Sensitivity study of the model to pyrite porosity

This analysis is performed for two extreme values of pyrite porosity – 5 % and 30 %. The velocities are calculated for the final model (not for step 4). The elastic wave velocities difference is less than 1 % as the porosity varies, which indicates their insensitivity to pyrite porosity changes. This can be explained by the fact that the overall volume concentration of pyrite is not high (no more than 17 %).

Sensitivity study of the model to matrix porosity

Figure 11 shows that the increasing matrix porosity mostly affects components C_{33} , C_{44} , and C_{11} . The other two moduli are less sensitive and exhibit only minor changes.

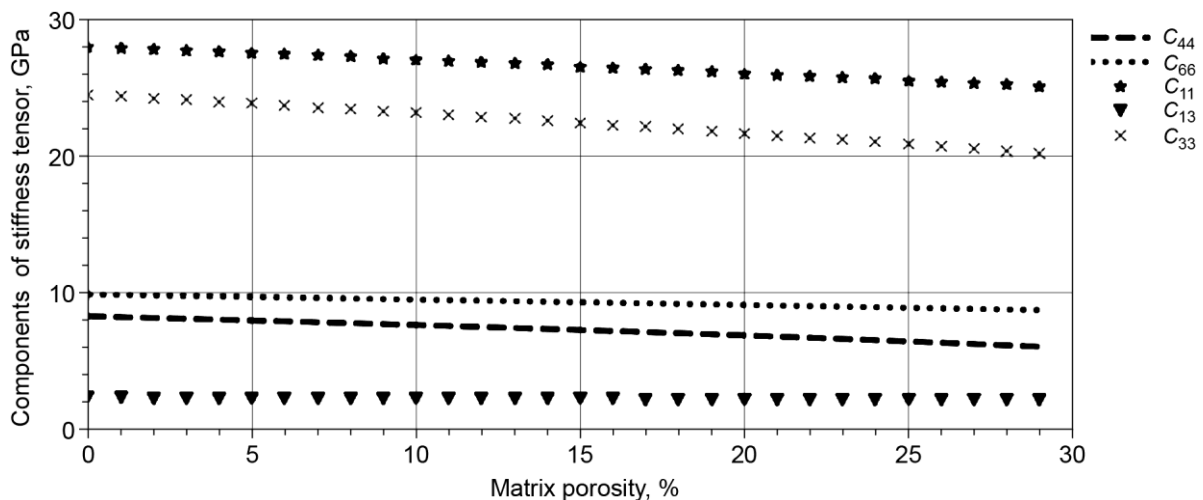


Fig. 11. Change in effective modules C_{ij} after 6th step due to matrix porosity increase at step 3

The model sensitivity to kerogen-filled radiolaria's skeletons inserted at step 5

The results of the sensitivity study are demonstrated in Figure 12. The maximum variation is seen for C_{11} (decreasing from 26.5 to 7 GPa). The moduli C_{11} and C_{33} drops almost twice as the concentration of kerogen-filled skeletons changes from 0 % to 50 %. The moduli C_{44} and C_{66} exhibit the least sensitivity, whereas the modulus C_{13} is insensitive to this parameter. In this part of sensitivity analysis, the radiolaria-related kerogen concentration increases while the volume concentration of the matrix (Material 3 + porous pyrite) decreases.

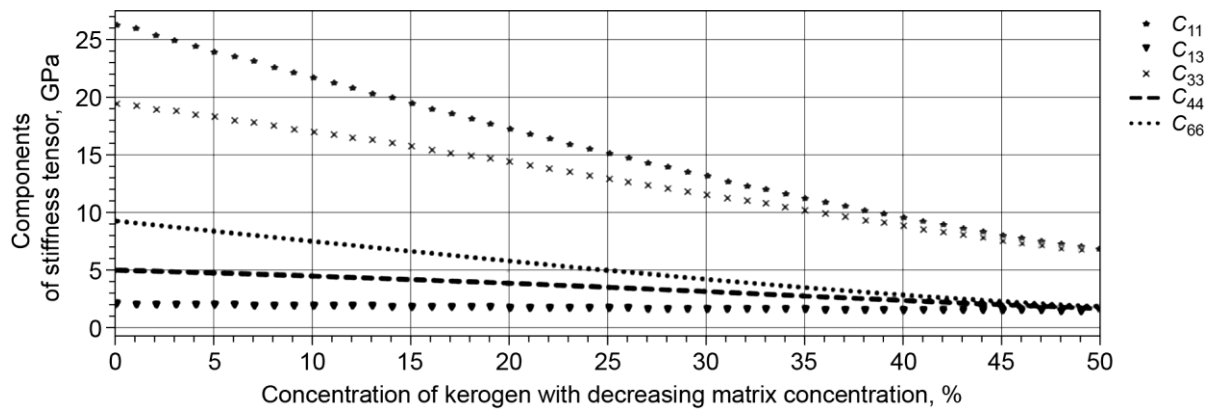


Fig. 12. Change in the effective moduli C_{ij} after 6th step with increasing volume concentration of the kerogen matrix at step 5. The volume concentrations of porous kerogen at respective step of modeling (2nd and 6th) are as follows: $v_2^k = 0.30$, $v_6^k = 0.05$

Sensitivity analysis for volume concentration of oriented elongated kerogen lenses

The lenses are considered as aligned thin layers, and the Backus method [Backus, 1962] is applied. The resulting medium has anisotropic elastic properties of VTI symmetry. Note that the anisotropy occurs in the model only at the final step 6.

The components of effective stiffness tensor versus the volume concentration of aligned kerogen layers are shown in Figure 13. The maximum change is seen for modulus C_{33} that decreases from 26.5 to 8.0 GPa as the layer's concentration increases from 0 % to 30 %. The decrease in C_{44} becomes less pronounced as the layer's concentration increases.

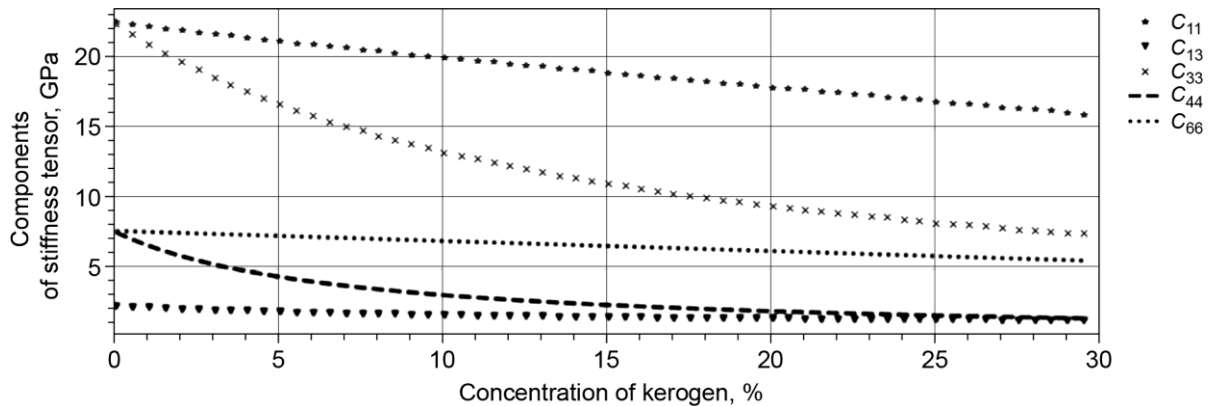


Fig. 13. Change in the effective moduli C_{ij} with the increasing volume concentration of the kerogen layers at step 6. The volume concentrations of porous kerogen at respective step of modeling (2nd and 5th) are as follows: $v_2^k = 0.30$, $v_5^k = 0.015$

Inversion of petroelastic model parameters from well log data

The petroelastic model of Bazhenov formation shale rocks and the method for construction of hierarchical volume model are applied to obtain the distribution of porosity between the matrix and kerogen, as well as the distribution of porous kerogen between the matrix and oriented layers. To determine these values, we use the well log data on the elastic wave velocities (V_P and V_S), density, total porosity, and volume concentration of the components.

First, solutions for the hierarchical volumetric model are found for the current depth with the help of algorithm described in the previous section. The set of solutions for concentrations c_{np} is used as input for the petroelastic model, and the effective elastic stiffness matrix is calculated for each particular solution. Then, the obtained components of the effective stiffness matrix are compared with their experimental analogs, calculated from the measured velocities and densities:

$$M_P = C_{33} = \rho V_P^2, \quad (18)$$

$$M_S = C_{44} = C_{55} = \rho V_S^2. \quad (19)$$

The values M_P and M_S are often called as modulus of P -wave (or S -wave). The solution of the inverse problem is a set of coefficients c_{np} , which provides an acceptable misfit between the theoretical and experimental data. In this study, it is assumed that such a discrepancy should not exceed 20 %, which corresponds to a discrepancy in the velocities of elastic waves of no more than 10 %.

A restriction is imposed on the solutions. If the values of the Thomsen parameters ε and γ calculated from the effective stiffness matrix exceed 0.8 the solution is considered as non-acceptable since the anisotropy is too high and never observed in experiments with rock samples (laboratory or field). The obtained solutions are classified depending on the residuals between the experimental and theoretical elastic moduli, which is controlled by the formula

$$\delta = 0.5 \sqrt{(\delta M_P)^2 + (\delta M_S)^2}, \quad (20)$$

where δM_P and δM_S are discrepancies in the wave moduli specified as a relative difference in the theoretical and experimental values of the respective modulus. The most probable solution for the current depth is a solution with the minimum residual.

Using the method of inverse problem solution described above we find the possible solutions for (a) kerogen in matrix versus kerogen in layers and (b) oil in kerogen versus oil in matrix. Kerogen in matrix is the sum of the first and second terms on the left-hand side of equation (8). The kerogen in layers is the third term on the left-hand side of this equation. The kerogen itself is assumed without pores. The oil in kerogen is the sum of the first and third terms in the left-hand side equation (9), and oil in matrix is the second term in the left-hand side of this equation.

Besides, an analysis of the sensitivity of elastic waves velocities to the distribution of kerogen between the matrix and layers and to the distribution of oil between the kerogen and matrix is carried out.

The values of residuals (20) when varying the kerogen distribution between the matrix and layers are shown in Fig. 14. Similar results for the residuals when varying the oil volume concentration between the matrix and kerogen are shown in Fig. 15. The total kerogen content and total oil porosity for a depth of 3075.7 meters, according to the mineral-component model, are 0.129 and 0.15, respectively.

Analyzing the results shown in the figures, we can conclude that there is a wide area of mutual combinations “kerogen in pores – kerogen in layers” and “oil in kerogen – oil in matrix”, providing solutions within the given limiting value of the residual (20) which is as high as 0.141. This value corresponds to the discrepancy between the theoretical and experimental elastic wave velocities 10 %. The width of this area depends on the specified level of acceptable residual. However, the pronounced variations in the residual values from smaller to larger ones make it possible to divide the area of solutions according to the degree of their reliability. Involvement of additional independent information obtained on cores (for example, studying the degree of anisotropy of elastic properties or estimating the range of porosity in kerogen) will narrow the area of the possible solutions.

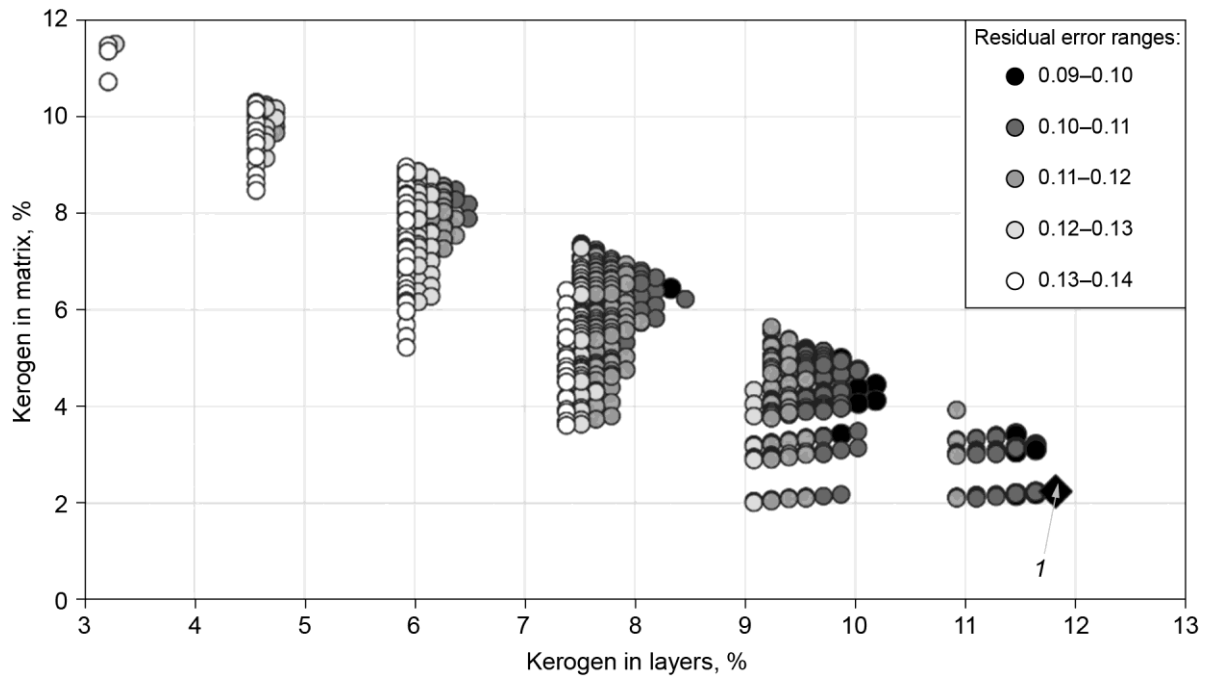


Fig. 14. Kerogen in matrix versus kerogen in layers for a depth of 3075.7 m (*1* – the most probable solution). The pores are filled with oil

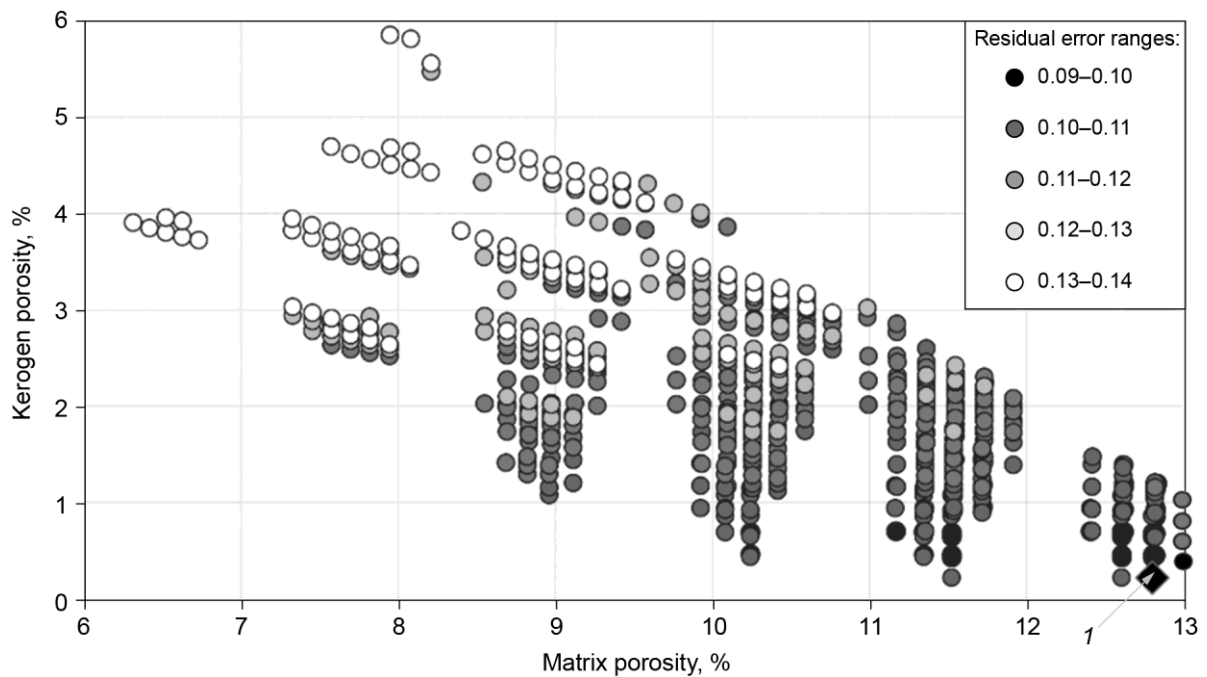


Fig. 15. Porosity in kerogen versus porosity in matrix for a depth of 3075.7 m (*1* – the most probable solution). The pores are filled with oil

Figures 16 and 17 show the dependences of compressional and shear wave velocities with increasing concentration of (a) kerogen in layers and (b) kerogen porosity for a specific depth (3075.7 meters). These dependences are provided by a set of forward problem solutions corresponding to the rock composition at this depth for different values of the model parameters.

Note that the total kerogen content and porosity is fixed in this analysis. Model velocities respond to changes in the concentration of kerogen layers and to redistribution of porosity between kerogen and matrix. As seen, the velocities of elastic waves decrease both with concentra-

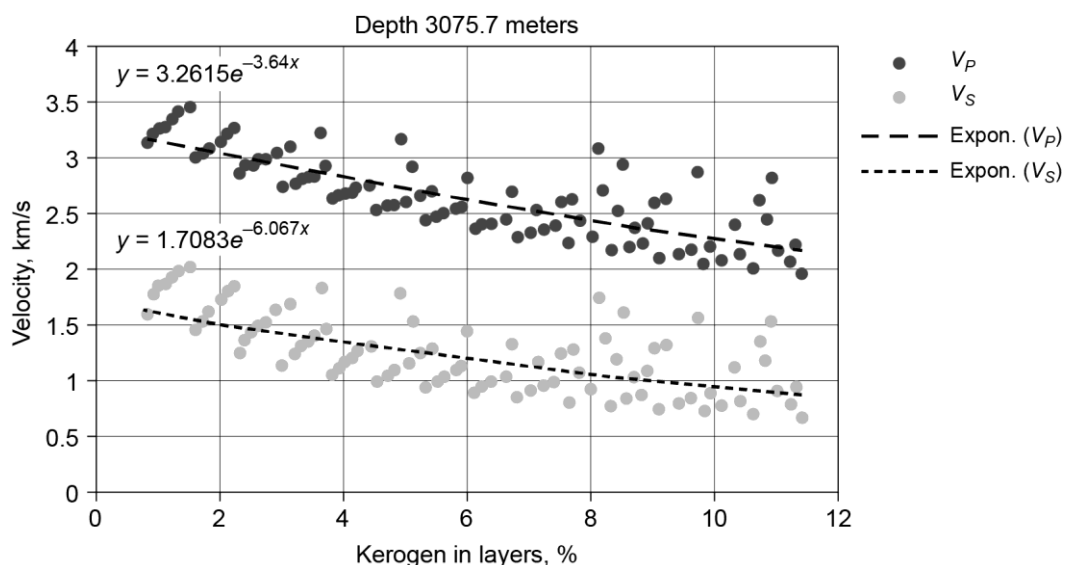


Fig. 16. Dependences of the velocities of compressional and shear waves on the concentration of kerogen layers. Total kerogen content is fixed. The trends are shown in black dotted lines

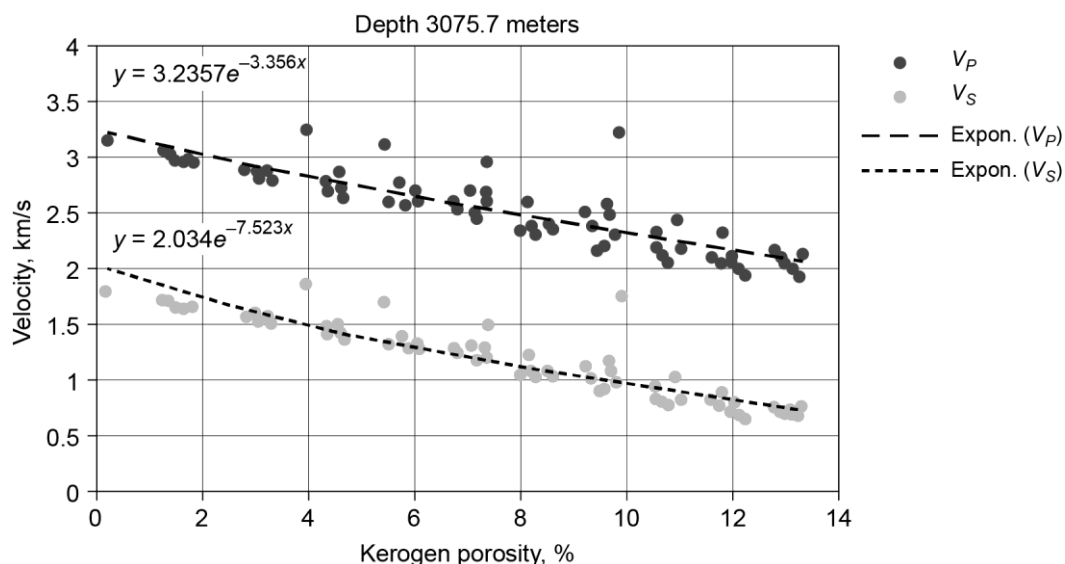


Fig. 17. Dependences of the velocities of compressional and shear waves on the kerogen porosity. Total porosity is fixed. The trends are shown in black dotted lines

tion of the kerogen layers and kerogen porosity. Moreover, the velocity of compressional wave can decrease by 1.5 times, and the shear wave velocity can even decrease by 4 times!

A comparison of theoretical and experimental velocities in the depth intervals 3045.5–3047.25 and 3074–3076 meters is shown in Figures 18 and 19. These are the depth intervals of kerogen-rich rocks. As seen, the theoretical and experimental velocities are in good agreement. It is interesting that the best agreement is observed for the shear waves. The maximum difference in velocities of 0.13 km/s is observed for compressional waves. Moving to results, Figures 18 and 19 shows that high kerogen porosity intervals highly correlate with lower velocities which is also justified by sensitivity study results. Components C_{33} and C_{44} are more affected by increase in kerogen porosity rather than an increase in the matrix porosity (Figures 7 and 11). The increase in concentration of kerogen in layers reflects in higher values of Thomsen parameters γ and ε . Note that parameter δ is practically constant over the depth interval. Also there is some noticeably tendency for only depth interval 3045.5–3047.25 with the increasing kerogen in layers the porosity in kerogen is becoming lower.

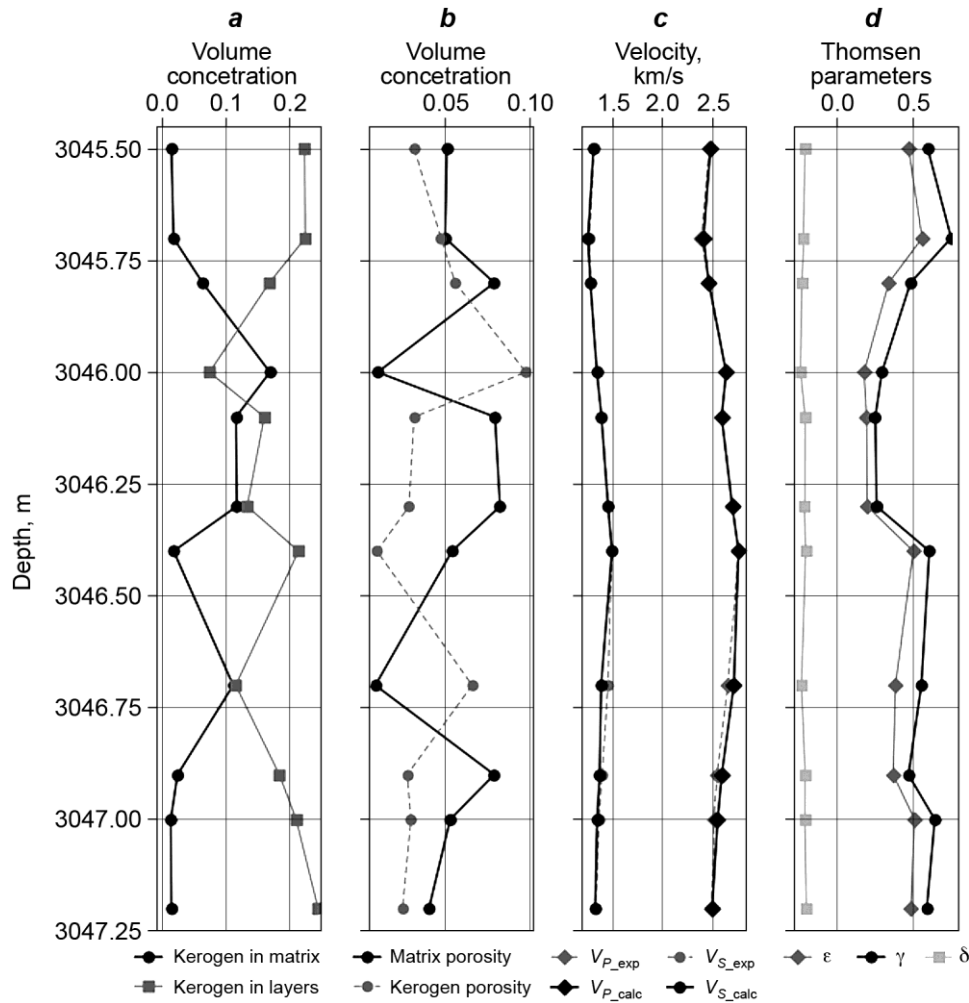


Fig. 18. *a, b* – solutions for kerogen (*a*) and porosity distribution (*b*) obtained from inversion; *c* – experimental (exp) vs calculated (calc) velocities of compressional and shear waves; *d* – Thomsen parameters for depth interval 3045.5–3047.25 m

Discussion and conclusions

In this work, a hierarchical petroelastic model of a shale reservoir represented by rocks of the Bazhenov formation is built. The goal of the model construction is to analyze how the distribution of kerogen between two forms: (a) kerogen as isometric inclusions in the mineral matrix and (b) kerogen as elongated layers in the matrix affects the elastic properties of the rocks – moduli and velocities. Similar analysis is performed for the distribution of oil porosity between the mineral matrix and kerogen. The model is constructed in several steps going from small to larger inclusions with taking into account a complex multiscale microstructure of studied rocks.

The construction of multistep model is reasonable since we show that a simple one-step model produces significantly overestimated velocities. Thus, the V_P and V_S found with the one-step model are almost 1.6 times greater than the velocities for multistep model. Such complicated models commonly have many parameters and some of them are unknown and even hard to be measured. Therefore, of importance is to carry out a sensitivity study of such a model in order to have an opportunity to fix some parameters. In the sensitivity study it is found that the model does not react to the aspect ratio of clay particles and kerogen. This can be explained by that the clay and kerogen content is not too large in this rock attaining 27 % and 19 %, respectively. This allows us to fix the aspect ratio of clay and kerogen particle.

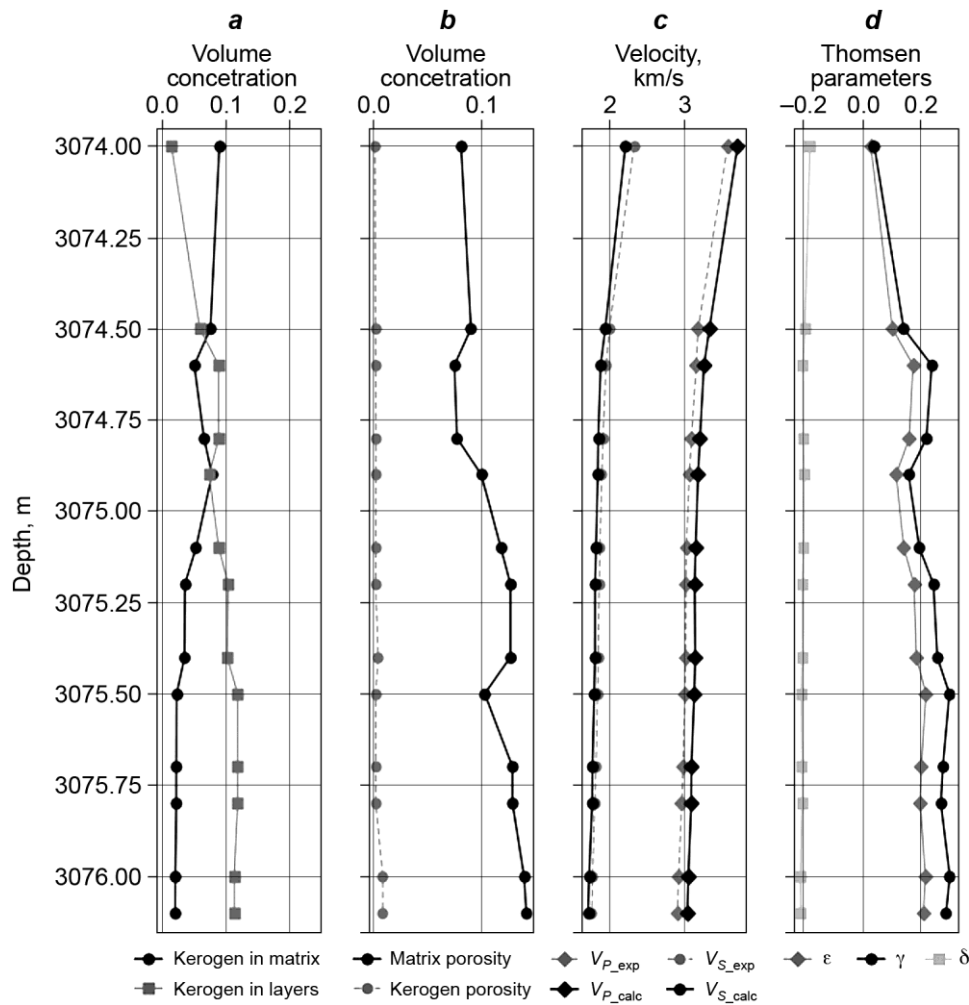


Fig. 19. Same as in Figure 18 but for depth interval 3074–3076 m

To simplify our calculations, we assume that their shape is spherical, however, we understand that this is not true for clay. Besides, to simplify our analysis, we neglect the intrinsic anisotropy of clay minerals. When studying the reasons of shale anisotropy, it should be taken into account but we have another goal in this study.

A construction of the hierarchical petroelastic is accompanied by a respective hierarchical volume model. This allows us to analyze the following dependencies:

- 1) volume concentration of kerogen in the matrix versus volume concentration of kerogen in layers;
- 2) kerogen porosity versus matrix porosity for pores filled with oil.

Depending on the form of kerogen occurrence (in matrix or in layers), the velocities of compressional waves can differ by 1.5 times, and shear ones by 4 times. With an increase in the porosity of kerogen up to 13% at a fixed total porosity, the velocities of compressional waves can decrease by 1.5 times, and the velocities of shear waves can decrease by half.

The developed petroelastic model is applied to well logging data in order to obtain all possible solutions for combinations “kerogen in matrix – kerogen in layers” and “oil porosity in matrix – oil porosity in kerogen” for two depths intervals containing shale rocks. The most probable solutions are also found for each logging depth. The constructed model approximates the experimental data with acceptable accuracy and can be used to predict the velocities of the Bazhenov formation shale rocks from their microstructure and vice versa – invert the experimental data on elastic wave velocities for distribution of kerogen between matrix and layers and distribution of porosity between the mineral matrix and kerogen.

Financial support

This work is performed in accordance with the State task of Schmidt Institute of Physics of the Earth of Russian Academy of Sciences.

Ethics declarations

The authors declare no conflict of interest.

References

- Ahrens T.J. Global Earth Physics: A Handbook of Physical Constants. Washington, DC: American Geophysical Union, 1995. 376 p.
- Backus G.E. Long-wave elastic anisotropy produced by horizontal layering // J. Geophys. Res. 1962. V. 67, Iss. 11. P.4427–4440. <https://doi.org/10.1029/JZ067i011p04427>
- Balushkina N.S., Kalmykov G.A. Cavity structure in oil saturated Bazhenov and Abalak shale rock in the Western Siberian Basin // Moscow Univ. Geol. Bull. 2016. V. 71, Iss. 1. P.71–80. <https://doi.org/10.3103/S0145875215050026>
- Balushkina N.S., Kalmykov G.A., Khamidullin R.A., Belokhin V.S., Korobova N.I., Petrakova N.N., Bakay A.I. Complex lithophysical typization of Bazhenov formation rocks from core analysis and well logging // SPE Russian Oil and Gas Exploration and Production Technical Conference and Exhibition, Moscow, 14–16 October 2014. <https://doi.org/10.2118/171168-MS>
- Bandyopadhyay K. Seismic anisotropy: geological causes and its implications to reservoir geophysics: PhD thesis. Stanford, CA: University of Stanford, 2009. 254 p.
- Bayuk I.O., Tikhotskiy S.A. Upscaling and downscaling of reservoir rock elastic properties: Rock physics approach // SEG Technical Program Expanded Abstracts. 2018. P.3653–3657. <https://doi.org/10.1190/segam2018-2985365.1>
- Bayuk I.O., Ammerman M., Chesnokov E.M. Elastic moduli of anisotropic clay // Geophysics. 2007. V. 72, N 5. P.D107–D117. <https://doi.org/10.1190/1.2757624>
- Bayuk I.O., Ammerman M., Chesnokov E.M. Upscaling of elastic properties of anisotropic sedimentary rocks // Geophys. J. Int. 2008. V. 172, Iss. 2. P.842–860. <https://doi.org/10.1111/j.1365-246X.2007.03645.x>
- Bayuk I.O., Danko D.A., Kulapova M.V., Ryzhkov V.I. Anisotropic rock-physics modeling of hadum rocks of Eastern and Central Ciscaucasia // Geofizika (Geophysics). 2019. V. 6. P.36–47. [in Russian].
- Belikov B.P., Aleksandrov K.S., Ryzhova T.V. Uprugie svoistva porodobrazuyushchikh mineralov i gornykh porod (Elastic Constants of Rock-forming Minerals). Moscow: Nauka, 1970. 276 p.
- Berge P.A., Berryman J.G. Realizability of negative pore compressibility in poroelastic composites // J. Appl. Mech. 1995. V. 62, Iss. 4. P.1053–1062. <https://doi.org/10.1115/1.2896042>
- Berryman J.G. Long-wavelength propagation in composite elastic media // J. Acoust. Soc. Amer. 1980. V. 68, Iss. 6. P.1809–1819. <https://doi.org/10.1121/1.385171>
- Berryman J.G. Mixture theories for rock properties // Rock Physics and Phase Relations: A Handbook of Physical Constants / Ed. T.J. Ahrens. Washington, DC: American Geophysical Union, 1995. P.205–228.
- Chesnokov E., Bayuk I.O., Ammerman M. Determination of shale stiffness tensor from standard logs // Geophys. Prospecting. 2010. V. 58, Iss. 6. P.1063–1082. <https://doi.org/10.1111/j.1365-2478.2010.00864.x>
- Curtis C.D., Lipshie S.R., Oertel G., Pearson M.J. Clay orientation in some Upper Carboniferous mudrocks, its relationship to quartz content and some inferences about fissility, porosity and compactional history // Sedimentology. 1980. V. 27, Iss. 3. P.333–339. <https://doi.org/10.1111/j.1365-3091.1980.tb01183.x>
- Danko D., Bayuk I., Klyazhnikov D., Ryzhkov V. The use of an anisotropic petroelastic model for the study of the Bazhenov formation // SEG Technical Program Expanded Abstracts. 2017. P.3801–3805. <https://doi.org/10.1190/segam2017-17784649.1>

- Dræge A., Jakobsen M., Johansen T.A.* Rock physics modelling of shale diagenesis // *Petrol. Geosci.* 2006. V. 12, N 1. P.49–57. <https://doi.org/10.1144/1354-079305-665>
- Gamero-Diaz H., Miller C., Lewis R.* sCore: A classification scheme for organic mudstones based on bulk mineralogy // AAPG 2012 Southwest Section Meeting, Fort Worth, TX, 19–22 May 2012. Search and Discovery Article No. 40951. 18 p.
- Gipson M.* A study of the relations with depth, porosity and clay mineral orientation in Pennsylvanian shales // *J. Sediment. Petrology.* 1966. V. 36, N 4. P.888–903. <https://doi.org/10.1306/74D715B9-2B21-11D7-8648000102C1865D>
- Hornby B.E., Schwartz L.M., Hudson J.A.* Anisotropic effective-medium modeling of the elastic properties of shales // *Geophysics.* 1994. V. 59, N 10. P.1570–1583. <https://doi.org/10.1190/1.1443546>
- Jakobsen M., Hudson J.A., Johansen T.A.* T-matrix approach to shale acoustics // *Geophys. J. Int.* 2003. V. 154, Iss. 2. P.533–558. <https://doi.org/10.1046/j.1365-246X.2003.01977.x>
- Kalmykov G.A.* Stroenie bazhenovskogo neftegazonosnogo kompleksa kak osnova prognoza differentsirovannoy nefteproduktivnosti (The structure of the Bazhenov oil and gas complex as the basis for forecasting differentiated oil productivity): D.Sc. Thesis. Moscow: Lomonosov Moscow State University, 2016. 391 p.
- Kuster G.T., Toksöz M.N.* Velocity and attenuation of seismic waves in two-phase media; Part I, Theoretical formulations // *Geophysics.* 1974a. V. 39, N 5. P.587–606. <https://doi.org/10.1190/1.1440450>
- Kuster G.T., Toksöz M.N.* Velocity and attenuation of seismic waves in two-phase media; Part II, Experimental results // *Geophysics.* 1974b. V. 39, N 5. P.607–618. <https://doi.org/10.1190/1.1440451>
- Loucks R.G., Ruppel S.C.* Mississippian Barnett Shale: Lithofacies and depositional setting of a deep-water shale-gas succession in the Fort Worth Basin, Texas // *AAPG Bull.* 2007. V. 91, N 4. P.579–601. <https://doi.org/10.1306/11020606059>
- McSkimin H.J., Andreatch P., Jr., Thurston R.N.* Elastic moduli of quartz versus hydrostatic pressure at 25 and –195.8 °C // *J. Appl. Phys.* 1965. V. 36, Iss. 5. P.1624–1632. <https://doi.org/10.1063/1.1703099>
- Ortega J.A., Ulm F.-J., Abousleiman Y.* The effect of nanogranular nature of shale on their poroelastic behavior // *Acta Geotechnica.* 2007. V. 2, Iss. 3. P.155–182. <https://doi.org/10.1007/s11440-007-0038-8>
- Peselnick L., Robie R.A.* Elastic constants of calcite // *J. Appl. Phys.* 1963. V. 34, Iss. 8. P.2494–2495. <https://doi.org/10.1063/1.1702777>
- Sayers C.M.* The effect of kerogen on the elastic anisotropy of organic-rich shales // *Geophysics.* 2013. V. 78, N 2. P.D65–D74. <https://doi.org/10.1190/geo2012-0309.1>
- Speight J.* Shale Oil and Gas Production Processes. Oxford: Elsevier, 2020. 1031 p.
- Vasin R.N., Wenk H.-R., Kanitpanyacharoen W., Matthies S., Wirth R.* Elastic anisotropy modeling of Kimmeridge shale // *J. Geophys. Res. Solid Earth.* 2013. V. 118, Iss. 8. P.3931–3956. <https://doi.org/10.1002/jgrb.50259>
- Yan F., Han D.-H.* Measurement of elastic properties of kerogen // SEG Technical Program Expanded Abstracts. 2013. P.2778–2782. <https://doi.org/10.1190/segam2013-1319.1>
- Zhao L., Qin X., Han D.-H., Geng J., Yang Zh., Cao H.* Rock-physics modeling for the elastic properties of organic shale at different maturity stages // *Geophysics.* 2016. V. 81, N 5. P.D527–D541. <https://doi.org/10.1190/geo2015-0713.1>

About the authors

ТЯПКИНА Anastasia Igorevna – Lomonosov Moscow State University, Faculty of Geology, Russia, 119991, Moscow, Leninskie Gory 1. E-mail: kabdo88@mail.ru

BEREZINA Irina Aleksandrovna – Schmidt Institute of Physics of the Earth of the Russian Academy of Sciences, Russia, 123242, Moscow, ul. Bolshaya Gruzinskaya 10, bld. 1. E-mail: irene.berezina@gmail.com

KALMYKOV Georgy Aleksandrovich – Lomonosov Moscow State University, Faculty of Geology. Russia, 119991, Moscow, Leninskie Gory 1. E-mail: gera64@mail.ru

OKUNEVICH Vsevolod Stanislavovich – Schmidt Institute of Physics of the Earth of the Russian Academy of Sciences. Russia, 123242, Moscow, ul. Bolshaya Gruzinskaya 10, bld. 1. E-mail: vogeophys@mail.ru

BAYUK Irina Olegovna – Schmidt Institute of Physics of the Earth of the Russian Academy of Sciences. Russia, 123242, Moscow, ul. Bolshaya Gruzinskaya 10, bld. 1. E-mail: ibayuk@ifz.ru

Влияние пористости и распределения керогена на упругие свойства сланцевых пород баженовской свиты – петроупругое моделирование

А.И. Тяпкина¹, И.А. Березина², Г.А. Калмыков¹, В.С. Окуневич², И.О. Баяук²

¹ *Московский государственный университет им. М.В. Ломоносова, г. Москва, Россия*

² *Институт физики Земли им. О.Ю. Шмидта РАН, г. Москва, Россия*

Автор для переписки: И.О. Баяук, e-mail: ibayuk@yandex.ru

Поступила в редакцию 06.02.2025 г.; после доработки 10.02.2025 г.

Принята к публикации 12.02.2025 г.

Аннотация. Создана параметрическая петроупругая модель аргиллитоподобных, богатых керогеном пород баженовской свиты. Модель построена на основе результатов анализа и состава породы, полученных с помощью электронного сканирующего микроскопа, и минерально-компонентной модели, полученной на основе интерпретации данных скважинных исследований. Предлагаемая модель предполагает, что кероген может находиться в минеральной матрице в разных формах: изометричные включения и тонкие слои. Кроме того, модель позволяет распределить пористость между керогеном и минеральной матрицей. Анализ чувствительности модели к ее параметрам показывает, что распределение керогена между матрицей и слоями может привести к значительным изменениям скоростей упругих волн (до 1.5 раз для волн сжатия и до 4 раз для поперечных волн). Скорости также очень чувствительны к распределению пористости между керогеном и матрицей. Построенная петроупругая модель применяется для инвертирования распределения следующих параметров по данным ГИС: а) кероген в минеральной матрице; б) кероген в тонких слоях; в) пористость матрицы; г) керогеновая пористость.

Ключевые слова: физика горных пород, петроупругое моделирование, анизотропия, упругие свойства, баженовская свита, сланцы, пористость керогена, матричная пористость, нетрадиционные породы-коллекторы

Цитируйте эту статью как: Тяпкина А.И., Березина И.А., Калмыков Г.А., Окуневич В.С., Баяук И.О. Влияние пористости и распределения керогена на упругие свойства сланцевых пород баженовской свиты – петроупругое моделирование // Сейсмические приборы. 2025. Т. 61, № 1. С.14–35. <https://doi.org/10.21455/si2025.1-2>

Финансирование

Работа выполнена согласно государственному заданию Института физики Земли им. О.Ю. Шмидта РАН.

Конфликт интересов

Авторы заявляют об отсутствии конфликта интересов.

Сведения об авторах

ТЯПКИНА Анастасия Игоревна – Московский государственный университет им. М.В. Ломоносова, геологический факультет. Россия, 119991, г. Москва, ГСП-1, Ленинские горы, д. 1. E-mail: kabdo88@mail.ru

БЕРЕЗИНА Ирина Александровна – Институт физики Земли им. О.Ю. Шмидта РАН. Россия, 123242, г. Москва, ул. Большая Грузинская, д. 10, стр. 1. E-mail: irene.berezina@gmail.com

КАЛМЫКОВ Георгий Александрович – Московский государственный университет им. М.В. Ломоносова, геологический факультет. Россия, 119991, г. Москва, ГСП-1, Ленинские горы, д. 1. E-mail: gera64@mail.ru

ОКУНЕВИЧ Всеволод Станиславович – Институт физики Земли им. О.Ю. Шмидта РАН. Россия, 123242, г. Москва, ул. Большая Грузинская, д. 10, стр. 1. E-mail: vogeophys@mail.ru

БАЮК Ирина Олеговна – Институт физики Земли им. О.Ю. Шмидта РАН. Россия, 123242, г. Москва, ул. Большая Грузинская, д. 10, стр. 1. E-mail: ibayuk@ifz.ru